



Article

# Development of Highly Ultraviolet-Protective Polypropylene/TiO<sub>2</sub> Nonwoven Fiber

Md. Abu Hanif <sup>1,\*</sup>, Hyokyeong Shin <sup>1</sup>, Danbi Chun <sup>1</sup>, Hong Gun Kim <sup>1,2</sup>, Lee Ku Kwac <sup>1,2</sup>, Sang-Won Han <sup>3</sup>, Sung-Soo Kang <sup>1,2</sup> and Young Soon Kim <sup>1,\*</sup>

<sup>1</sup> Institute of Carbon Technology, Jeonju University, Jeonju 55069, Jeollabuk-do, Republic of Korea

<sup>2</sup> Graduate School of Carbon Convergence Engineering, Jeonju University, Jeonju 55069, Jeollabuk-do, Republic of Korea

<sup>3</sup> Sunjin Glotech Inc., Gimje 54353, Jeollabuk-do, Republic of Korea

\* Correspondence: hanif21@jj.ac.kr (M.A.H.); kyscjb@jj.ac.kr (Y.S.K.); Tel.: +82-63-220-3157 (Y.S.K.)

**Abstract:** In recent decades, there has been a rise in public consciousness of the adverse effects of expanded skin contact with sunlight, particularly the ultraviolet (UV) spectrum. UV radiation causes serious health problems like skin cancer, early aging, erythema, pigmentation, etc., due to contact with the skin. Therefore, the highly efficient UV-protection materials were manufactured using polypropylene and TiO<sub>2</sub> (PPTO) through cost-effective and easy methods. The designated 7.5 PPTO and 15 PPTO were prepared, varying the amount of TiO<sub>2</sub>, as well as without using TiO<sub>2</sub> (PPNF), which was also manufactured as a control material. All the as-synthesized nonwoven fibers were carefully characterized employing a variety of microscopic and spectroscopic methods, such as X-ray diffraction, Fourier transform infrared spectroscopy, thermogravimetric analysis, field-emission scanning electron microscopy, energy-dispersive X-ray spectroscopy, ultraviolet–visible diffuse reflectance spectroscopy, and contact angle measurements. In conclusion, 15 PPTO showed the highest UV-protection ability (87.5%) compared to 7.5 PPTO and PPNF. In addition, 15 PPTO exhibited 1.76 and 1.32 times higher protection than 7.5 PPTO and PPNF, respectively, when exposed to UB-B radiation. The enhanced activity may be due to the amount of TiO<sub>2</sub> because TiO<sub>2</sub> increased the product's absorption and reflection capability. Overall, the PPTO nonwoven fibers can be applied to block harmful UV radiation.



**Citation:** Hanif, M.A.; Shin, H.; Chun, D.; Kim, H.G.; Kwac, L.K.; Han, S.-W.; Kang, S.-S.; Kim, Y.S. Development of Highly Ultraviolet-Protective Polypropylene/TiO<sub>2</sub> Nonwoven Fiber. *J. Compos. Sci.* **2024**, *8*, 86. <https://doi.org/10.3390/jcs8030086>

Academic Editor: Francesco Tornabene

Received: 23 December 2023

Revised: 2 February 2024

Accepted: 23 February 2024

Published: 25 February 2024



**Copyright:** © 2024 by the authors. Licensee MDPI, Basel, Switzerland. This article is an open access article distributed under the terms and conditions of the Creative Commons Attribution (CC BY) license (<https://creativecommons.org/licenses/by/4.0/>).

**Keywords:** polypropylene; titanium dioxide; nonwoven fiber; UV protection

## 1. Introduction

Scientists have been paying more attention to ultraviolet (UV) radiation (280~400 nm) over the past decade due to the higher amounts of UV entering the top of the planet as a result of the loss of ozone in the stratosphere. The range of wavelengths of the sunlight's radiation is roughly 0.7–3000 nm. Nevertheless, only a portion of this electromagnetic radiation, which ranges from 280 to 3000 nm, reaches the earth's surface; UV radiation makes up a portion of this spectrum between 100 and 400 nm [1]. Long-term sunlight exposure causes erythema, pigmentation, sunburn, early aging, and skin cancer. In the meantime, UV-A (315~400 nm) and UV-B (280~315 nm) radiation pose a greater threat to the well-being of humans [2]. This is because a portion of UV-B and UV-C in the atmosphere of the globe are blocked by the protective ozone layer. The top of the earth is now receiving more UV rays as a result of the ozone barrier being thinner. Since the outermost layer of skin is the biggest organ in the body, it shields the wearer from ultraviolet radiation. UV irradiation results in the destruction of DNA and photochemical reactions that occur [3]. According to epidemiological investigations, carcinoma of the skin probability is raised by unintentional or intentional contact with sunlight at work. In Europe, between 29 and 51% of those who handle potentially dangerous substances also have been in contact with UV

radiation (UVR). Approximately ten percent of UVR, or two to nine times more, is received by outdoor workers than by interior workers [4]. Thus, safeguarding employees against UV radiation is crucial for their health, especially for those who spend a lot of time outside in the sun all over the world.

In the last few decades, nanotechnologies have significantly contributed to the fabrication of technologically sophisticated textiles by enhancing their chemical and physical characteristics and prolonging their lifespan [5]. Furthermore, the incorporation of nanomaterials into the manufacturing of smart textiles confers upon fabrics' additional valuable attributes, like water-resistant, UV protection, and antimicrobial, all without compromising the fabrics' tactility, lightness, flexibility, and breathability. Numerous industries, including medicine, pharmaceuticals, human reproduction, sports, environment, and electronics, have found extensive uses for smart textiles treated with nanoparticles [6].

Currently, a wide range of polypropylene (PP) textile goods are accessible, including clothing, covers, upholstery fabrics, and technical textiles. The low cost, ease of manufacturing, low density, high tensile strength, and superior chemical stability of PP textile goods make them the favored option. PP does have certain drawbacks, too, including low polarity, UV stability, and heat stability [7,8]. When unstabilized PP is used as a fiber, then it is highly vulnerable to degradation by sunlight. Antioxidants and UV stabilizing substances, therefore, become necessary to safeguard the polymer both during usage and storage facilities. Notwithstanding the fact that PP fibers deteriorate when exposed to UV radiation in the presence of air oxygen, PP textile goods with various UV stabilization and UV blocking qualities are currently marketable.

Textiles can be utilized as UV-protective materials if they are finished properly and have the right light absorbers. One way to change textile fabrics for UV protection is to utilize inorganic and organic particles as fillers. Because they are nontoxic and chemically stable to UV radiation at high temperatures, inorganic UV blockers like  $\text{TiO}_2$ ,  $\text{ZnO}$ , and  $\text{SiO}_2$  are preferred over organic UV blockers [9].  $\text{TiO}_2$  and  $\text{ZnO}$  are two of these inorganic UV blockers that are frequently utilized. Due to consumer demands, the UV-protection capabilities of textiles coated with nanoparticles have received a lot of attention nowadays. By absorbing and preventing UV light from penetrating a fabric, these materials can offer protection from it. The coating of  $\text{TiO}_2$  on the fabric produced excellent UV protection [10]. UV-absorbing materials should be bonded to the fibers with strong covalent bonds for long-lasting effects. Specific pigments that are present, like titanium dioxide ( $\text{TiO}_2$ ), can be added to the fiber substance of fibers made from synthetic materials throughout the manufacturing procedure to provide long-lasting UV protection [11–13].

There has been more research lately regarding how nanoparticles can alter the characteristics of polymeric textile fibers and fabrics [14–17]. Nanoparticles can generally be added to textile materials using two basic methods: either the nanoparticles are applied to the textiles during finishing procedures, or they are incorporated into the textile strands themselves. Common coating techniques have already been used to apply nanosized  $\text{TiO}_2$  to fiber assemblies [17]. It has been found that nanosized  $\text{TiO}_2$  is more effective than standard-size  $\text{TiO}_2$  at both absorbing and scattering UV rays, making it a more effective UV blocker.

The present research focused on the development of high-performance UV-protective nonwoven fiber. We prepared polypropylene/ $\text{TiO}_2$  (PPTO) nonwoven fiber using PP pellet and nanosized  $\text{TiO}_2$  by easy, economical, and inexpensive compounding and melt-blown techniques. In this work, 7.5 and 15%  $\text{TiO}_2$  were used to synthesize the PPTO products. In addition, polypropylene nonwoven fiber (PPNF) was prepared as a control experiment without using  $\text{TiO}_2$ . Among the as-synthesized materials,  $\text{TiO}_2$ -containing compounds showed good UV-protection ability, and 15%  $\text{TiO}_2$  materials provided the highest UV-blocking capability. These excellent results might be due to the reflecting and absorbing UV light ability of  $\text{TiO}_2$ . To the best of our knowledge, no previous reports have been made regarding a comparable method for manufacturing PPTO nonwoven fiber and similar work.

## 2. Materials and Methods

### 2.1. Materials

Polypropylene pellet (99.8%, MFI: 1100 g 10 min<sup>-1</sup>) was purchased from Sunjin Glotech, Inc., Jeollabuk-do, Republic of Korea. TiO<sub>2</sub> nanoparticles (particle size ~50 nm) were received from Sukgyung AT Co., Ltd., Ansan, Republic of Korea.

### 2.2. Preparation of Polypropylene/TiO<sub>2</sub> Nonwoven Fiber

The polypropylene/TiO<sub>2</sub> nonwoven fiber was prepared by a simple two-step process: compounding and conventional melt-blown. In the first step, 92.5% and 85% polypropylene pellet compounding with 7.5% and 15% TiO<sub>2</sub> additives were used, respectively, to obtain a homogeneous polypropylene/TiO<sub>2</sub> pellet. This compounding method is an important stage in the growth of polymers and is usually carried out in the state of molten form with the aim of achieving a homogenous blend. In the final step, the polypropylene/TiO<sub>2</sub> pellet was used to prepare polypropylene/TiO<sub>2</sub> nonwoven fiber using the conventional melt-blown method. Figure 1 shows the representative diagram for the production of polypropylene/TiO<sub>2</sub> nonwoven fiber. The obtained polypropylene/TiO<sub>2</sub> nonwoven fiber prepared using 7.5% and 15% TiO<sub>2</sub> were designated as 7.5 PPTO and 15 PPTO, respectively. Polypropylene nonwoven fiber was synthesized as a control experiment without using TiO<sub>2</sub> and named PPNF. In this case, only the one-step conventional melt-blown method was applied.

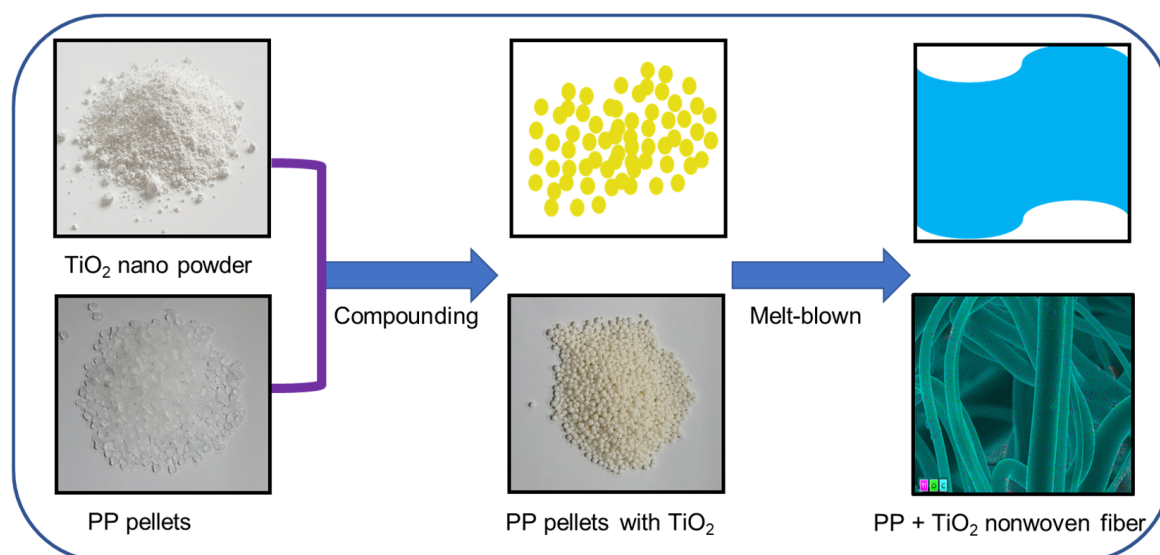


**Figure 1.** Schematic illustration of the synthesis of polypropylene/TiO<sub>2</sub> nonwoven fiber.

### 2.3. Characterization

X-ray diffractometer (XRD, X'Pert PRO, PANalytical) equipped with a Cu K $\alpha$  ( $\lambda = 1.5406 \text{ \AA}$ ) radiation source was used to analyze the crystal structure of the samples. Fourier transform infrared (FTIR, Thermo Fisher Scientific (Waltham, MA, USA), Nicolet iS5) spectroscopy was applied for the investigation of the functional groups present in the compounds. To examine the thermal properties of the as-prepared samples, thermogravimetric analysis (TGA) and derivative thermogravimetric (DTG) (SDT Q600) TA instrument (Universal V4.5 A TA Instruments, New Castle, DE, USA) were used. The morphological analysis of the compounds was examined using field-emission scanning electron microscopy (FE-SEM) and energy-dispersive X-ray spectroscopy (EDS). The ultraviolet–visible diffuse reflectance spectroscopy (UV–Vis DRS, Perkin Elmer Lambda 25, Ayer Rajah, Singapore) was used to measure the optical properties and bandgaps of the materials. The water contact angle of the products was inspected by applying Phoenix 300 Touch (SEO Co., Ltd., Pyeongtaek, Republic of Korea).

#### 2.4. Measurements of UV-Protection Ability

The UV-protection ability of the TiO<sub>2</sub>, 7.5 PPTO, and 15 PPTO was tested using a UV-VIS-NIR spectrophotometer (PerkinElmer Lambda 1050 with 150 mm InGaAs integrating sphere) according to KS K 0850:2019, and the measurement was conducted at a wavelength interval of 5 nm in a wavelength range of 280 to 400 nm. The samples were kept for 4 h under the standard atmosphere ( $20 \pm 2.0$ ) °C and relative humidity ( $65 \pm 4.0$ )% during the experiment. Prior to testing, the samples should be conditioned until equilibrium is reached by leaving the nonwoven fiber in the area where the test is to be performed so that air can flow freely through the environment of the nonwoven fiber. The  $5 \times 5$  cm<sup>2</sup> size of the nonwoven fiber was used to investigate the UV-protection ability. The test was conducted under the standard condition of ( $20 \pm 2.0$ ) °C and relative humidity ( $65 \pm 4.0$ )%. The scan speed for ultraviolet irradiation was  $923.59 \text{ nm min}^{-1}$ , maintained during the UV-protection rate measurements. The spectrophotometer is calibrated as follows:

- The wavelength is corrected using a holmium oxide filter, which is a filter for ultraviolet wavelengths, as an absorption band filter.
- The transmission linearity is corrected with a calibrated mesh with a transmission close to 6.7%, 3.3%, and 2.0%.

After that, the sample was placed directly in front of the integrating sphere for UV protection testing at 5 nm intervals in the 280–400 nm wavelength range. We analyzed the nonwoven fiber at three different wavelength ranges: UV-R (280–400 nm), UV-A (315–400 nm), and UV-B (280–315 nm). The representative sample image is shown in Figure 2. Four consecutive runs of the tests were conducted in order to assess the precision of the findings.



Figure 2. The as-prepared PPNF, 7.5 PPTO, and 15 PPTO products.

### 3. Results and Discussion

#### 3.1. Structural Properties

The structural properties of the TiO<sub>2</sub>, 7.5 PPTO, and 15 PPTO were analyzed using X-ray diffraction (XRD). The XRD spectra of the samples are shown in Figure 3. Two different XRD phases are visible in TiO<sub>2</sub>: anatase and rutile phase. The anatase phases of the (101), (004), (200), (105), and (211) planes are responsible for the diffraction peaks at  $2\theta$  angles of  $25.32^\circ$ ,  $37.80^\circ$ ,  $47.98^\circ$ ,  $53.92^\circ$ , and  $55.09^\circ$  (JCPDS card No. 96–500-0224), respectively [18]. However, the rutile phases of the (110) and (101) planes are attributed to  $27.44^\circ$  and  $36.07^\circ$  (JCPDS Card No. 21-1276), respectively [19]. The 7.5 PPTO and 15 PPTO samples exhibit all of the characteristic peaks of TiO<sub>2</sub> along with the diffraction peaks at  $2\theta$  angles of  $14.21^\circ$ ,  $16.79^\circ$ ,  $18.36^\circ$ , and  $21.42^\circ$  which can be attributed to the  $\alpha$ -form (PP) of crystal planes (110), (040), (130), and (060), in that order [20]. The TiO<sub>2</sub> peaks do not clearly seem in the 15 PPTO sample due to all the high-intensity polypropylene peaks of the 15 PPTO sample, and the TiO<sub>2</sub> peak intensity is comparatively low. The substances have diminished their appearance of being crystalline and now possess a highly ordered lamellar structure. A similar result was noted in the case of an oriented polypropylene sample. The addition of TiO<sub>2</sub> does not appear to change the diffraction angles in any noticeable way.

Consequently, it was shown that the addition of TiO<sub>2</sub> did not affect the structure of the crystals of the polypropylene framework.

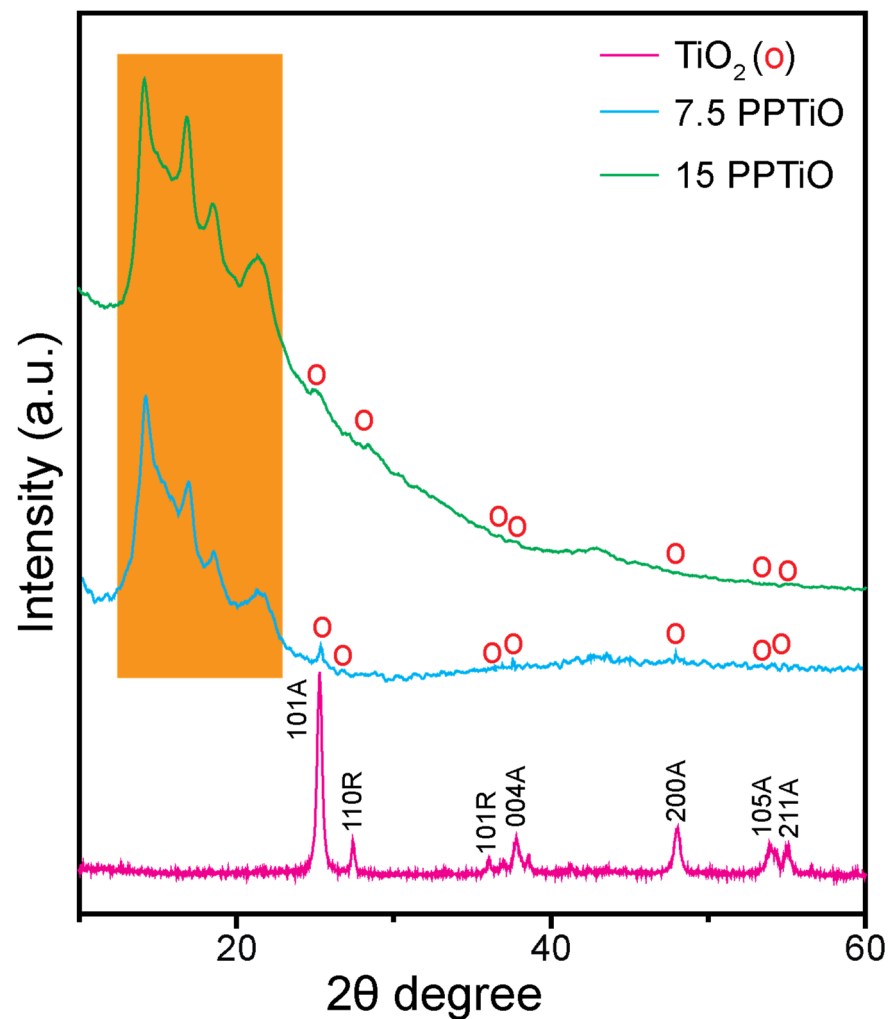


**Figure 3.** XRD Spectra of TiO<sub>2</sub>, 7.5 PPTO, and 15 PPTO.

Further, Fourier transform infrared spectroscopy (FTIR) was applied to explore the bonding characteristics and functional groups of TiO<sub>2</sub>, PPNF, 7.5 PPTO, and 15 PPTO, and the representative spectra were shown in Figure 4. The peak observed in TiO<sub>2</sub> at around 565 cm<sup>-1</sup> can be attributed to vibrations in the Ti–O stretching mode. Furthermore, a large peak at 3200 to 3500 cm<sup>-1</sup> and peaks at 1643 cm<sup>-1</sup> corresponds to the stretching and bending vibrations of O–H from surface-adsorbed water molecules, respectively [20,21]. The symmetric bending of –CH<sub>3</sub> and the bending vibration of –CH<sub>2</sub> are linked to the PP peaks at 1374 and 1455 cm<sup>-1</sup>, respectively. Additionally, the peaks at 2837 and 2873 cm<sup>-1</sup> are identified for the –CH<sub>3</sub> and –CH<sub>2</sub> symmetric stretching vibrations. The peaks located at 2916 and 2952 cm<sup>-1</sup> are responsible for the asymmetrical vibrations of stretching of –CH<sub>3</sub> and –CH<sub>2</sub>, respectively [22]. In the 7.5 PPTO and 15 PPTO samples, all of the characteristic peaks of both PP and TiO<sub>2</sub> were detected in the spectrum, indicating that 7.5 PPTO and 15 PPTO had been successfully prepared. We may conclude that the inclusion of TiO<sub>2</sub> had no effect on the bonding environment of the PP atmosphere. These outcomes agree with the findings of the XRD.

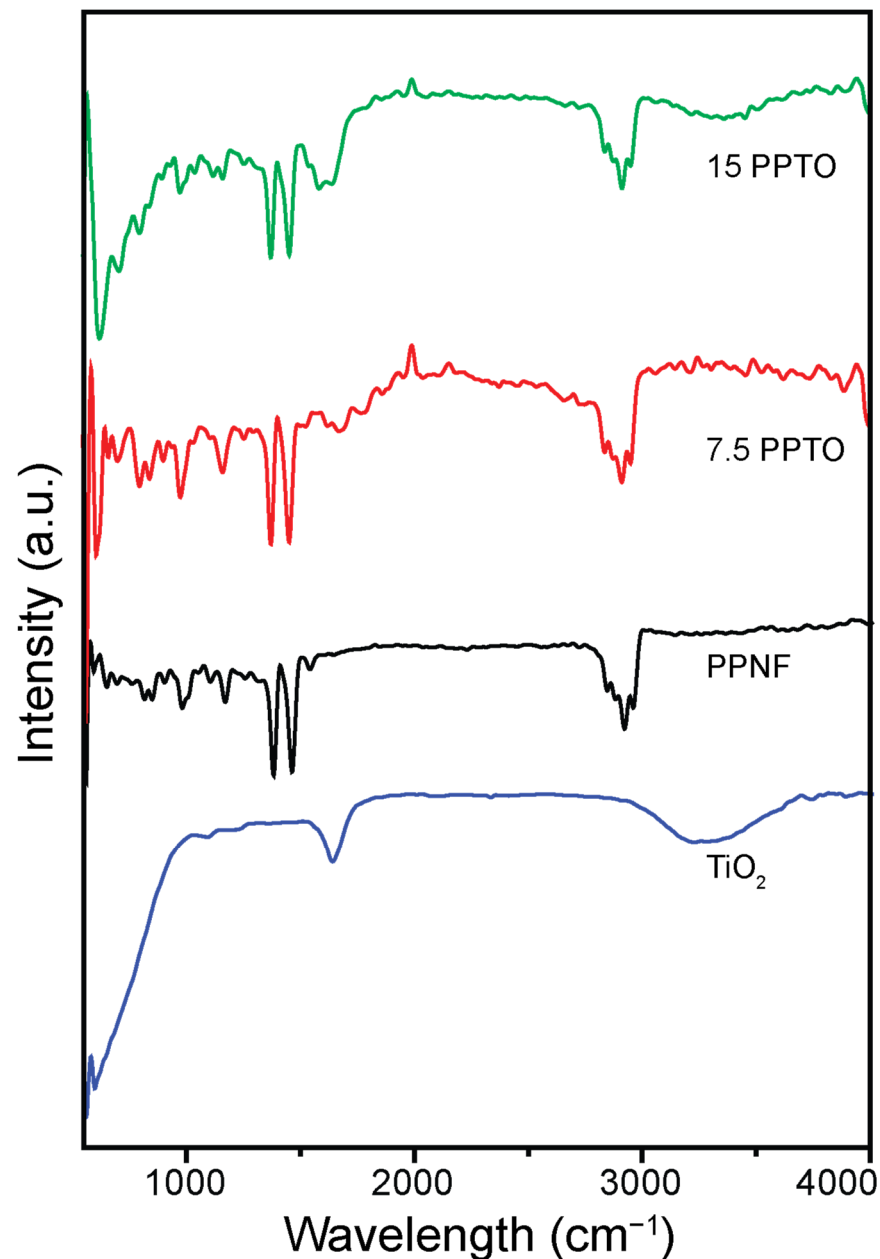


**Figure 4.** FTIR spectra of TiO<sub>2</sub>, PPNF, 7.5 PPTO, and 15 PPTO.

### 3.2. Thermal Properties

The thermal characteristics of PPNF, 7.5 PPTO, and 15 PPTO were examined using TA instruments in a nitrogen (N<sub>2</sub>) atmosphere, with a heating rate of 10 °C/min and a temperature range of 50 to 800 °C. The samples' TGA and DTG curves are shown in Figure 5. All the samples underwent distinct stages of thermal degradation following thermal evaluation at temperatures as high as 800 °C. Figure 5a shows that there were two weight-loss stages for all the investigated samples. The first weight reduction was observed in the range 150–295 °C, and the second was 295–419 °C. There was no more weight loss after heating up to 800 °C. Figure 5b also confirmed that there were two similar decomposition regions in the DTG curves. The results indicated that the 15 PPTO showed a lower decomposition rate compared to 7.5 PPTO and PPNF. It might be due to the presence of a higher amount of TiO<sub>2</sub> in the 15 PPTO material. Also, it has been explained by the TiO<sub>2</sub>, which acts as a kind of barrier to stop the transmission of heat and prohibit the samples

from melting down. In addition, the weight loss of PPNF and 7.5 PPTO are greater than 15 PPTO, which confirms the 15 PPTO is more stable compared to PPNF and 7.5 PPTO.

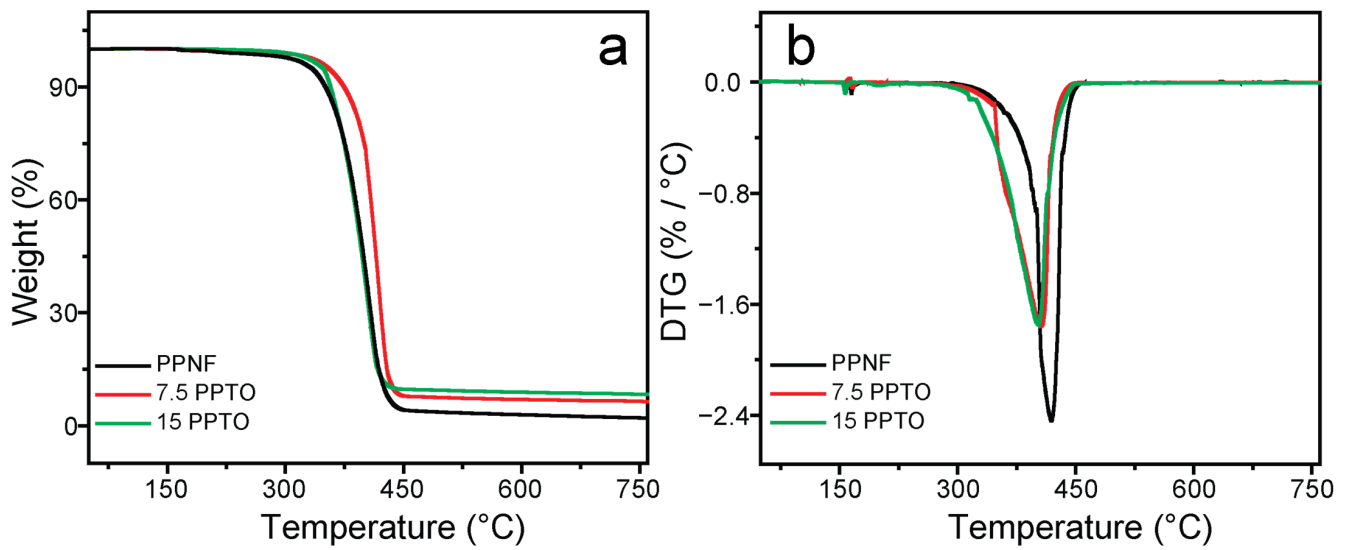


Figure 5. (a) TGA and (b) DTG spectra of PPNF, 7.5 PPTO, and 15 PPTO.

### 3.3. Morphological Properties

The morphological analysis of PPNF, 7.5 PPTO, and 15 PPTO were conducted using FE-SEM and shown in Figure 6. It can be seen from Figure 6a–c that all the nonwoven fibers displayed interconnected open pore topologies with arbitrarily arranged microfibers. The average diameter and standard deviation (STDEV) of PPNF was  $2.79 \pm 1.25 \mu\text{m}$  (Figure 6a). In addition, the surface and shape of PPNF was almost smooth and uniform. After the addition of 7.5%  $\text{TiO}_2$ , the average diameter of the nonwoven fiber reduced slightly, and the average diameter was  $2.28 \pm 1.30 \mu\text{m}$  (Figure 6b). The amount of  $\text{TiO}_2$  increased up to 15% and found the thinnest diameter. The average diameter of 15 PPTO was  $1.56 \pm 0.83 \mu\text{m}$  (Figure 6c). ImageJ software (ImageJ 1.46r) was used to measure the diameter of products. Therefore, the FE-SEM analysis indicated that  $\text{TiO}_2$  plays a crucial role in reducing the diameter. Interestingly, the  $\text{TiO}_2$  nanoparticles are not visible on the surface of PPNF because of our unique manufacturing process (compounding and melt-blown method).

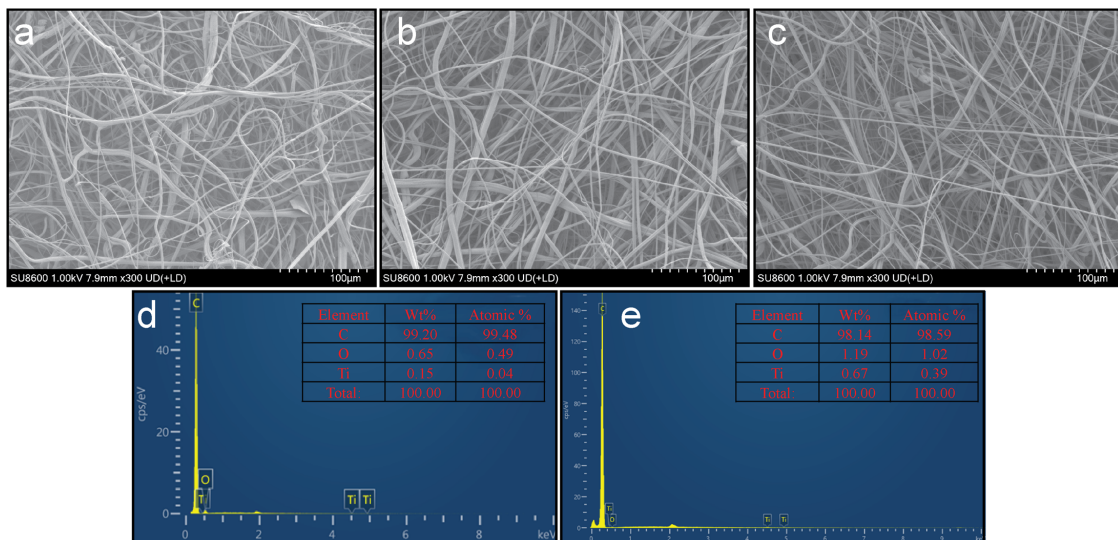
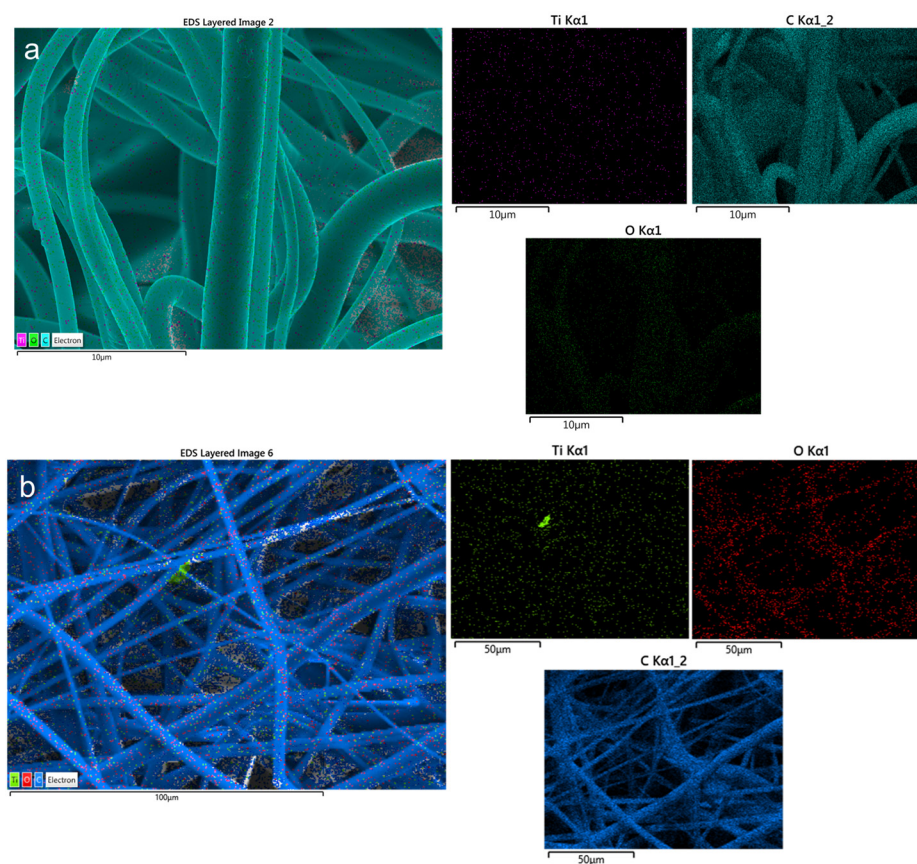


Figure 6. FE-SEM image of (a) PPNF, (b) 7.5 PPTO, and (c) 15 PPTO. EDS spectra of (d) 7.5 PPTO and (e) 15 PPTO.

Moreover, the EDS analysis was applied to ensure the presence of TiO<sub>2</sub> nanoparticles in 7.5 PPTO and 15 PPTO systems. Figure 6d,e showed the corresponding EDS results confirming the three representative elements Ti, O, and C. These outcomes confirm the existence of TiO<sub>2</sub> nanoparticles. Also, it is clearly shown that with the increases in TiO<sub>2</sub> nanoparticles, the atomic and weight percentages of titanium and oxygen are increased. On the other hand, the amount of carbon is decreased, respectively. Therefore, the TiO<sub>2</sub> nanoparticles were inserted into the PP pellet successfully.

Furthermore, the elemental mapping analysis was used to determine the elemental distribution of 7.5 and 15 PPTO in order to provide more insight, and the data are shown in Figure 7. Both the compounds were perfectly formed by the combination of polypropylene and TiO<sub>2</sub>, as evidenced by the existence of the three representative elements (C, Ti, and O) and the lack of any other elements (Figure 7a,b).



**Figure 7.** Elemental mapping analysis of (a) 7.5 PPTO and (b) 15 PPTO.

### 3.4. Wettability Measurement

Wettability depends on the substances' chemical constitution and geometrical architecture. The wettability of the material was assessed using roll-off angles and static contact angles (CA). It is challenging to obtain precise numbers for the advancing and receding water CA due to the protruding fibers' elasticity and strain on the water droplet [23]. Therefore, the wettability of PPNF, 7.5 PPTO, and 15 PPTO were measured using only static CA. We performed the water CA experiment five times and calculated the average water CA of the samples. The digital photograph images of the shape of water droplets during CA measurement are shown in Figure 8a–c. In addition, Table 1 displays the wettability of all the investigated samples as determined by measuring the contact angle. The average water CA of PPNF was  $(129.49 \pm 1.62)^\circ$ , showing hydrophobic properties. This value exceeds the commonly reported value, which is approximately  $80^\circ$  on smooth polyester (PET) films [24,25]. In contrast, the water CA is enhanced with the addition of TiO<sub>2</sub> nanoparticles. The increasing order of water CA was

PPNF ( $129.49 \pm 1.62$ )° < 7.5 PPTO ( $136.59 \pm 2.84$ )° < 15 PPTO ( $141.73 \pm 4.18$ )°. Therefore, 15 PPTO showed higher hydrophobicity compared to 7.5 PPTO and PPNF due to the higher amount of TiO<sub>2</sub> present in the 15 PPTO compound. In line with additional findings published in the literature, the existence of oxide form in the polymer matrix enhanced the hydrophobicity compared to the polymer alone [26–28]. Thus, water resistance and UV blocking qualities would be included in this material, which would be created using a technique different from the conventional nanoparticle impregnation or coating processes.

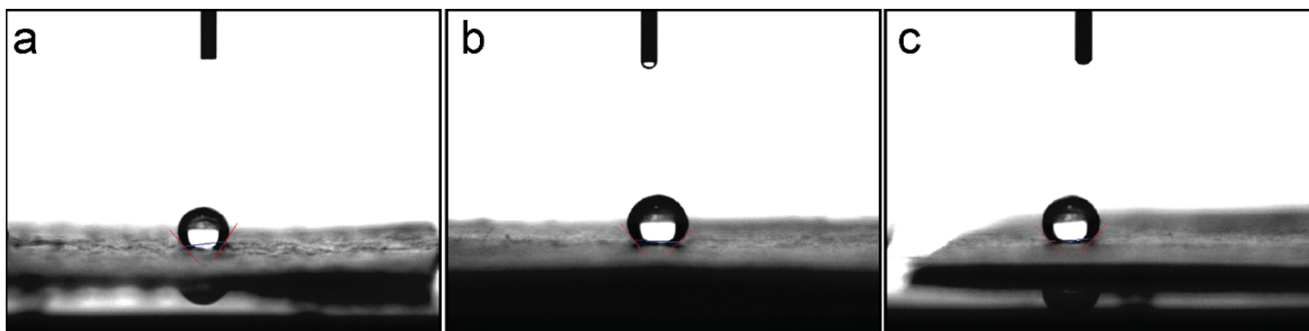


**Figure 8.** Contact angle measurement of (a) PPNF, (b) 7.5 PPTO, and (c) 15 PPTO.

**Table 1.** The static water contact angle of PPNF, 7.5 PPTO, and 15 PPTO with standard deviation (STDEV).

Serial No.	Sample Name, CA		
	PPNF, $\theta$ (°)	7.5 PPTO, $\theta$ (°)	15 PPTO, $\theta$ (°)
1st run	131.65	136.40	145.30
2nd run	127.03	136.89	146.02
3rd run	130.81	141.60	141.32
4th run	129.17	135.04	134.24
5th run	128.79	133.01	141.77
Average + STDEV	$129.49 \pm 1.62$	$136.59 \pm 2.84$	$141.73 \pm 4.18$

### 3.5. UV-Protection Analysis

The optical properties of the material are the most important parameter for investigating the UV-protection ability. Therefore, the optical properties of the PPNF, 7.5 PPTO, and 15 PPTO were analyzed using the UV-Vis DRS technique and shown in Figure 9. According to the acquired spectra, all the analyzed samples' visible light absorbance in the region (>400 nm) is still incredibly low, while their light absorbance across the UV region (280~400) is high, providing a vital need for an efficient UV screening agent [29]. Figure 9a indicates that 15 PPTO exhibit high absorbance intensity in both the UV-B (280~315 nm) and UV-A (315~400 nm) wavelength regions. In addition, the UV absorbance of 15 PPTO is greater than that of the PPNF and 7.5 PPTO compounds in both the designated area and the absorbance increasing order: PPNF < 7.5 PPTO < 15 PPTO. These prominent outcomes might be the amount of TiO<sub>2</sub>. The absorbance increases in line with the increase in TiO<sub>2</sub>. It is found that the 15 PPTO nonwoven fiber may block only UV radiation effectively with a wavelength of less than approximately 400 nm. Furthermore, according to UV-Vis DRS data, the UV-protection ability will be improved in the UV-B region compared to the UV-A region due to the higher absorbance efficiency in that UV-B area for the representative materials.

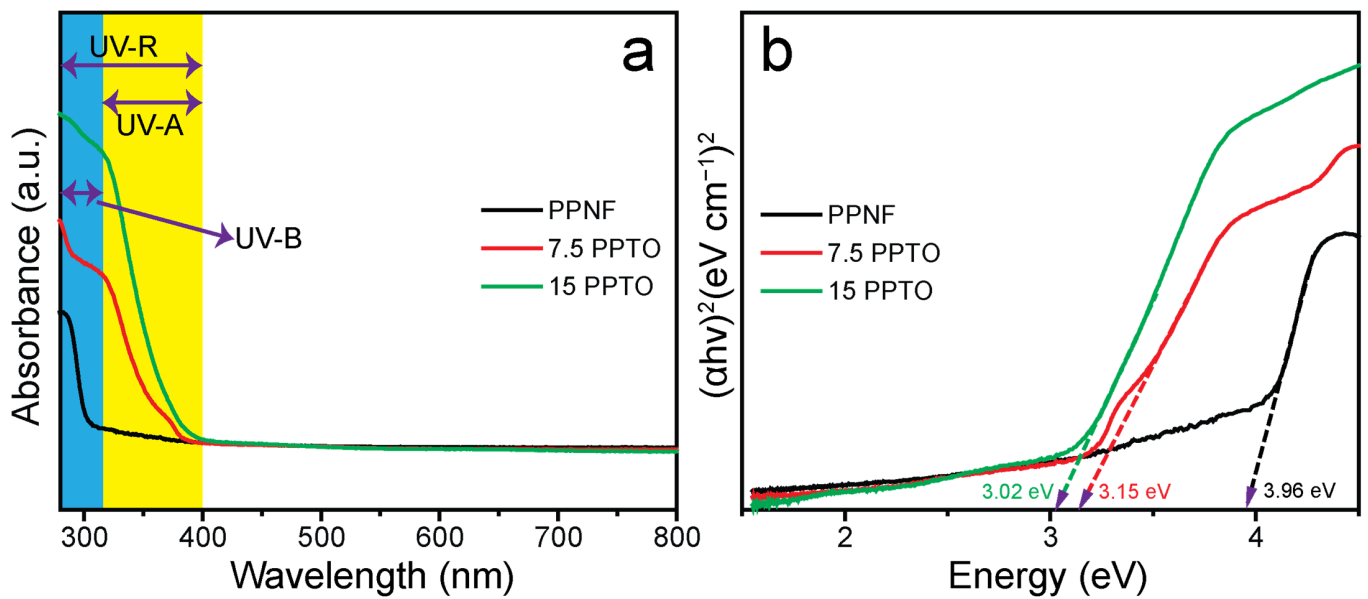


**Figure 9.** (a) UV-Vis DRS spectra of PPNF, 7.5 PPTO, and 15 PPTO and (b) Tauc plots of PPNF, 7.5 PPTO, and 15 PPTO.

Additionally, in order to elucidate the optical behavior of the analyzed materials, Tauc’s plots and the following Equation (1) are utilized to calculate the bandgap energy of PPNF, 7.5 PPTO, and 15 PPTO compounds:

$$(\alpha h\nu)^n = A (h\nu - E_g) \tag{1}$$

where  $h$  signifies the Planck constant,  $\nu$  refers to the photon’s frequency,  $A$  represents the constant, and  $E_g$  denotes bandgap energy. The properties of the electron transition determine the value of  $n$ , where  $n = 0.5$  or  $2$  for indirect or direct transition, respectively. The representative absorption spectra were utilized to make Tauc plots. The  $E_g$  value was obtained by vertically extrapolating the straight line  $(\alpha h\nu)^2$  vs.  $E$  graph to the X-axis at  $(\alpha h\nu)^2 = 0$  (Figure 9b). The computed  $E_g$  value of PPNF, 7.5 PPTO, and 15 PPTO was 3.96, 3.15, and 3.02 eV, respectively. It was observed that the  $E_g$  value was decreased in the following order: PPNF > 7.5 PPTO > 15 PPTO, and 15 PPTO held the least bandgap energy. The materials under investigation were appropriate for application in optical UV-protecting equipment, and the bandgaps improved the light absorption properties. Additionally, the existence of unstructured defects, which raise the density of localized states in the bandgap, may be responsible for this bandgap drop, and the least bandgap energy material increased the UV-shielding ability [30].

UV-Vis transmission spectra were accounted for in the calculation of the UV-blocking performance. The UV radiation emitted by the sun falls into three wavelength bands, which are typically identified as UV-A (315~400 nm), UV-B (280~315 nm), and UV-C (100~280 nm). Nonetheless, only UV radiation with wavelengths between 290 and 400 nm can reach the earth’s surface because the stratospheric ozone in the earth’s atmosphere absorbs UVC and some UVB radiation [31]. Figure 10 shows the UV-Vis transmission spectra of PPNF, 7.5 PPTO, and 15 PPTO. The results indicated that the PPNF shows a higher transmission, which means PPNF provides lower UV-protection efficiency. Surprisingly, the transmission curve was decreased after the incorporation of TiO<sub>2</sub> nanoparticles into the PP pellets. The transmittance was gradually decreased from PPNF to 7.5 PPTO and finally reduced to 12.60% for 15 PPTO materials, which suggests that the higher amount of TiO<sub>2</sub>-containing products have excellent UV-protection ability. As far as we are aware, the TiO<sub>2</sub> nanoparticles worked well as a UV-protecting material, both reflecting and absorbing UV light. The obtained results suggest that the strong UV scattering and absorbance capabilities of

TiO<sub>2</sub> nanostructures, which are mainly revealed at the coatings' interface layer, may be responsible for their potency as UV-protective properties [32]. The TiO<sub>2</sub> nanoparticles minimized the amount of light transmitted while converting UV rays into heat and visible light [33].

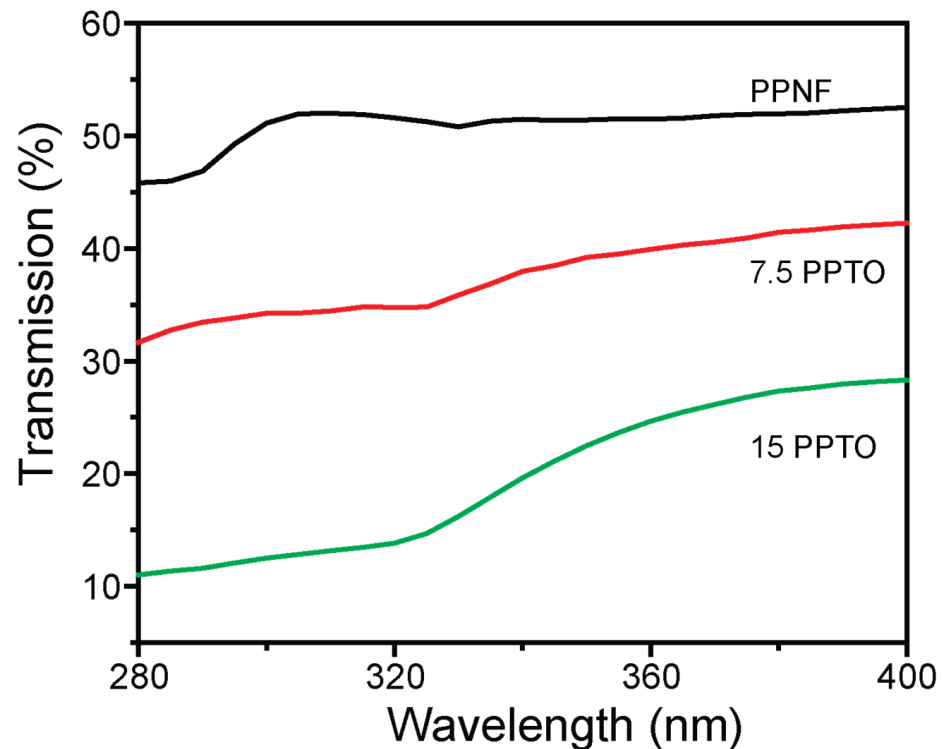


**Figure 10.** UV-Vis transmission spectra of PPNE, 7.5 PPTO, and 15 PPTO.

Table 2 shows the UV-protection ability of PPNE, 7.5 PPTO, and 15 PPTO. We analyzed the UV-protection ability at different wavelength regions, UV-A (315~400 nm) and UV-B (280~315 nm). The result indicates that all the products show excellent UV-protection ability in the UV-B region compared to UV-A, and among them, 15 PPTO demonstrate higher proficiency (87.4%) compared to 7.5 PPTO (65.8%) and PPNE (49.5%). The UV-blocking performance of all the investigated samples was also examined in the UVR (280~400 nm) region, and a remarkable result was found. All the samples were analyzed four times with identical conditions, and the average and standard deviation data are shown in Table 2.

**Table 2.** The UV-protection ability of PPNE, 7.5 PPTO, and 15 PPTO.

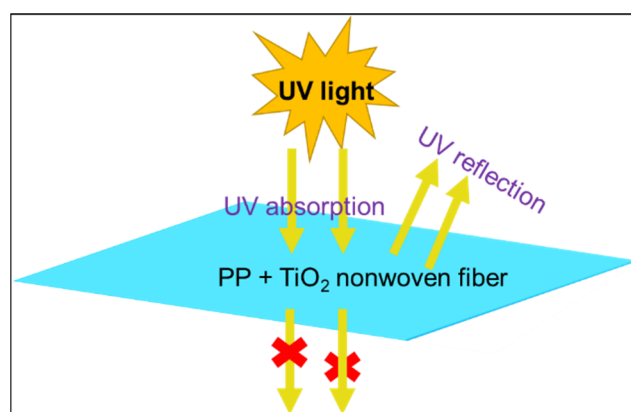
Wavelength	UV-Protection Ability (%)		
	PPNE	7.5 PPTO	15 PPTO
(280~400) UV-R	48.6 ± 0.44	62.0 ± 1.92	79.7 ± 1.18
(315~400) UV-A	48.3 ± 0.44	60.9 ± 1.86	77.5 ± 1.16
(280~315) UV-B	49.5 ± 0.45	65.8 ± 1.91	87.4 ± 1.24

Table 3 compares the UV-blocking efficiency of the best as-synthesized 15 PPTO product with previously reported polymer and metal oxide-based compounds. As can be seen from Table 3, the 15 PPTO shows a comparable finding. Therefore, PPTO nonwoven fiber can be used to shield from harmful UV radiation.

**Table 3.** Comparison of the UV-protection performance of polymer and metal oxide-based compounds.

Sample Name	UV-Protection Ability (%)			Ref.
	280 nm	320 nm	360 nm	
Ba doped TiO <sub>2</sub> nanoparticles	-	53	18	[34]
Al doped ZnO/Epoxy nanocomposite	50	45	40	[35]
PVA/CAN doped ZnO composite film	58	56	40	[36]
Cd doped CuO nanoparticles	64	70	76	[37]
Sn doped ZnO quantum dots	75	38	25	[38]
polymer and carbon/N doped ZnO nanomaterials	70	85	75	[39]
15 PPTO	88.99	86.18	75.34	Present Work

A simple UV-protection mechanism of PPTO nonwoven fiber is proposed and shown in Figure 11. This mechanism can be explained through the absorption and reflection of UV radiation from the surface of the nonwoven fiber. A wide variety of inorganic UV-absorber materials, such as ZnO or TiO<sub>2</sub>, is used to synthesize high-performance UV-blocking products. The present works deal with the production of highly active UV-shielding polypropylene + TiO<sub>2</sub> materials. It can be seen from Figure 11 that the UV-ray radiation could not pass through the as-synthesized nonwoven fiber, which might be the absorption or reflection of UV-rays by the surface of PPTO nonwoven fiber. This effect improves the product's ability to protect against UV rays coming from UV light sources.

**Figure 11.** The schematic diagram for the UV-protective mechanism using PPTO nonwoven fiber.

#### 4. Conclusions

In summary, the polypropylene/TiO<sub>2</sub> (PPTO) nonwoven fiber was manufactured by a modest two-step process: compounding and melt-blown. Different state-of-the-art techniques are used to methodically investigate the as-synthesized PPTO product. The FTIR and XRD data show that the PPNF's polypropylene crystal structure remained unchanged after TiO<sub>2</sub> NPs were added to the PP pellet. Also, the successful preparation of PPTO nonwoven fiber was confirmed. According to the thermogravimetric investigation, 15 PPTO is more stable compared to 7.5 PPTO and PPNF compounds, which makes the 15 PPTO material more effective. All the as-prepared nonwoven fiber has randomly organized microfibers in interconnecting open pore architectures. In addition, the UV absorbance of 15 PPTO is greater than that of the PPNF and 7.5 PPTO and follows the increasing order: PPNF < 7.5 PPTO < 15 PPTO. A significant amount of TiO<sub>2</sub> may be the cause of these notable results. The results show that only UV light with a wavelength of less than about 400 nm can be successfully blocked by the PPTO nonwoven fiber. The enhanced performance indicates that the effectiveness of TiO<sub>2</sub> nanostructures as UV-protective qualities may be attributed to their significant UV scattering and absorption abilities. Therefore, our as-synthesized products can be applied to protect the UV radiation in our daily lives. Specifically, it can be

suitable for a variety of practical applications such as oil/water separation, wall/vehicle glass coverings, polymer electret filters, truck liners, etc.

**Author Contributions:** Conceptualization, M.A.H. and Y.S.K.; methodology, M.A.H., Y.S.K. and S.-W.H.; software, M.A.H.; formal analysis, M.A.H., H.S., D.C., L.K.K., S.-S.K. and Y.S.K.; investigation, and data curation, M.A.H., H.S., D.C., S.-S.K. and S.-W.H.; writing—original draft preparation, M.A.H.; writing—review and editing, M.A.H. and Y.S.K.; supervision, L.K.K. and H.G.K.; project administration, H.G.K.; funding acquisition, H.G.K. All authors have read and agreed to the published version of the manuscript.

**Funding:** This study was supported by the National Research Foundation of Korea (NRF) grant funded by the Korean government (MSIT) (No.2016R1A6A1A03012069 and No.2020R1A2C1102174).

**Data Availability Statement:** The data presented in the paper are available upon request.

**Conflicts of Interest:** Sang-Won Han was employed by Sunjin Glotech Inc. The remaining authors declare that the research was conducted in the absence of any commercial or financial relationships that could be construed as a potential conflict of interest.

## References

1. Tian, M.; Hu, X.; Qu, L.; Du, M.; Zhu, S.; Sun, Y.; Han, G. Ultraviolet Protection Cotton Fabric Achieved via Layer-by-layer Self-assembly of Graphene Oxide and Chitosan. *Appl. Surf. Sci.* **2016**, *377*, 141–148. [[CrossRef](#)]
2. Mavrić, Z.; Tomšič, B.; Simončič, B. Recent advances in the ultraviolet protection finishing of textiles. *Tekstilec* **2018**, *61*, 201–220. [[CrossRef](#)]
3. González, S.; Fernández-Lorente, M.; Gilaberte-Calzada, Y. The latest on skin photoprotection. *Clin. Dermatol.* **2008**, *26*, 614–626. [[PubMed](#)]
4. Xin, J.H.; Daoud, W.A.; Kong, Y.Y. A new approach to UV-blocking treatment for cotton fabrics. *Text. Res. J.* **2004**, *74*, 97–100. [[CrossRef](#)]
5. Yetisen, A.K.; Qu, H.; Manbachi, A.; Butt, H.; Dokmeci, M.R.; Hinstroza, J.P.; Skorobogatiy, M.; Khademhosseini, A.; Yun, S.H. Nanotechnology in textiles. *ACS Nano* **2016**, *10*, 3042–3068. [[CrossRef](#)] [[PubMed](#)]
6. Alhashmi Alamer, F.; Beyari, R.F. The Influence of Titanium Oxide Nanoparticles and UV Radiation on the Electrical Properties of PEDOT:PSS-Coated Cotton Fabrics. *Materials* **2023**, *16*, 1738. [[CrossRef](#)] [[PubMed](#)]
7. Karian, H. *Handbook of Polypropylene and Polypropylene Composites, Revised and Expanded*; CRC Press: Boca Raton, FL, USA, 2003.
8. Lewin, M. *Handbook of Fiber Chemistry*, 3rd ed.; Taylor & Francis Group: Boca Raton, FL, USA, 2006; pp. 812–958.
9. Khan, M.Z.; Taghavian, H.; Fijalkowski, M.; Militky, J.; Tomkova, B.; Venkataraman, M.; Adach, K. Effect of microwave power on bactericidal and UV protection properties of the ZnO nanorods grown cotton fabrics. *Colloids Surf. A Physicochem. Eng. Asp.* **2023**, *664*, 131135. [[CrossRef](#)]
10. Khan, M.Z.; Ashraf, M.; Hussain, T.; Rehman, A.; Malik, M.M.; Raza, Z.A.; Nawab, Y.; Zia, Q. In situ deposition of TiO<sub>2</sub> nanoparticles on polyester fabric and study of its functional properties. *Fibers Polym.* **2015**, *16*, 1092–1097. [[CrossRef](#)]
11. Bogdan, J.; Jackowska-Tracz, A.; Zarzyńska, J.; Pławińska-Czarnak, J. Chances and limitations of nanosized titanium dioxide practical application in view of its physicochemical properties. *Nanoscale Res. Lett.* **2015**, *10*, 57. [[CrossRef](#)] [[PubMed](#)]
12. Topcu, S.; Jodhani, G.; Gouma, P. Optimized Nanostructured TiO<sub>2</sub> Photocatalysts. *Front. Mater.* **2016**, *3*, 35. [[CrossRef](#)]
13. Fernández-Domene, R.M.; Sánchez-Tovar, R.; Sánchez-González, S.; García-Antón, J. Photoelectrochemical characterization of anatase-rutile mixed TiO<sub>2</sub> nanosponges. *Int. J. Hydrogen Energy* **2016**, *41*, 18380–18388. [[CrossRef](#)]
14. Catone, D.L. Raw Materials-Nano-particle additives for PET. *Chem. Fibers Int.* **2004**, *54*, 25.
15. Rottstegge, J.; Zhang, X.; Zhou, Y.; Xu, D.; Han, C.C.; Wang, D. Polymer nanocomposite powders and melt spun fibers filled with silica nanoparticles. *J. Appl. Polym. Sci.* **2007**, *103*, 218–227. [[CrossRef](#)]
16. Erdem, N.; Cireli, A.A.; Erdogan, U.H. Flame retardancy behaviors and structural properties of polypropylene/nano-SiO<sub>2</sub> composite textile filaments. *J. Appl. Polym. Sci.* **2009**, *111*, 2085–2091. [[CrossRef](#)]
17. Han, K.; Yu, M. Study of the preparation and properties of UV-blocking fabrics of a PET/TiO<sub>2</sub> nanocomposite prepared by in situ polycondensation. *J. Appl. Polym. Sci.* **2006**, *100*, 1588–1593. [[CrossRef](#)]
18. Akter, J.; Hanif, M.A.; Islam, M.A.; Sapkota, K.P.; Hahn, J.R. Selective growth of Ti<sup>3+</sup>/TiO<sub>2</sub>/CNT and Ti<sup>3+</sup>/TiO<sub>2</sub>/C nanocomposite for enhanced visible-light utilization to degrade organic pollutants by lowering TiO<sub>2</sub>-bandgap. *Sci. Rep.* **2021**, *11*, 9490. [[CrossRef](#)] [[PubMed](#)]
19. Lee, C.H.; Rhee, S.W.; Choi, H.W. Preparation of TiO<sub>2</sub> nanotube/nanoparticle composite particles and their applications in dye-sensitized solar cells. *Nanoscale Res. Lett.* **2012**, *7*, 48. [[CrossRef](#)]
20. Hanif, M.A.; Shin, H.; Chun, D.; Kim, H.G.; Kwac, L.K.; Kim, Y.S. Photocatalytic VOCs Degradation Efficiency of Polypropylene Membranes by Incorporation of TiO<sub>2</sub> Nanoparticles. *Membranes* **2023**, *13*, 50. [[CrossRef](#)]
21. Kumar, R.; Ahmed, M.; Bhadrachari, G.; Al-Mesri, A.; Thomas, J. A Facile Approach of Thin Film Coating Consisted of Hydrophobic Titanium Dioxide over Polypropylene Membrane for Membrane Distillation. *J. Membr. Sci.* **2019**, *6*, 196–202.

22. Sun, F.; Li, T.-T.; Ren, H.; Jiang, Q.; Peng, H.-K.; Lin, Q.; Lou, C.-W.; Lin, J.-H. PP/TiO<sub>2</sub> Melt-Blown Membranes for Oil/Water Separation and Photocatalysis: Manufacturing Techniques and Property Evaluations. *Polymers* **2019**, *11*, 775. [[CrossRef](#)]
23. Li, H.; Zhang, H.; Hu, J.-J.; Wang, G.-F.; Cui, J.-Q.; Zhang, Y.-F.; Zhen, Q. Facile Preparation of Hydrophobic PLA/PBE Micro-Nanofiber Fabrics via the Melt-Blown Process for High-Efficacy Oil/Water Separation. *Polymers* **2022**, *14*, 1667. [[CrossRef](#)] [[PubMed](#)]
24. Topala, I.; Dumitrascu, N.; Pohoata, V. Influence of plasma treatments on the hemocompatibility of PET and PET+ TiO<sub>2</sub> films. *Plasma Chem. Plasma Process.* **2008**, *28*, 535–551. [[CrossRef](#)]
25. Placinta, G.; Arefi-Khonsari, F.; Gheorghiu, M.; Amouroux, J.; Popa, G. Surface properties and the stability of poly(ethylene terephthalate) (PET) films treated in plasmas of He–O<sub>2</sub> mixtures. *J. Appl. Polym. Sci.* **1997**, *66*, 1367–1376. [[CrossRef](#)]
26. Wu, J.; Xia, J.; Jing, C.; Lei, W.; Wang, B.P. Formation of hierarchical ZnO nanostructure on tinfoil substrate and the application on wetting repellency. *Appl. Phys. A* **2011**, *105*, 221–224. [[CrossRef](#)]
27. Shaik, U.P.; Kshirsagar, S.; Krishna, M.G.; Tewari, S.P.; Dhar Purkayastha, D.; Madhurima, V. Growth of superhydrophobic zinc oxide nanowire thin films. *Mater. Lett.* **2012**, *75*, 51–53. [[CrossRef](#)]
28. Li, J.; Yang, Y.; Zha, F.; Lei, Z. Facile fabrication of superhydrophobic ZnO surfaces from high to low water adhesion. *Mater. Lett.* **2012**, *75*, 71–73. [[CrossRef](#)]
29. Tsuzuki, T.; He, R.; Wang, J.; Sun, L.; Wang, X.; Hocking, R. Reduction of the photocatalytic activity of ZnO nanoparticles for UV protection applications. *Int. J. Nanotechnol.* **2012**, *9*, 1017–1029. [[CrossRef](#)]
30. Bouzidi, A.; Jilani, W.; Yahia, I.S.; Zahran, H.Y.; Assiri, M.A. Optical Analysis and UV-Blocking Filter of Cadmium Iodide-Doped Polyvinyl Alcohol Polymeric Composite Films: Synthesis and Dielectric Properties. *J. Inorg. Organomet. Polym. Mater.* **2020**, *30*, 3940–3952. [[CrossRef](#)]
31. Algaba, I.; Riva, A. In vitro measurement of the ultraviolet protection factor of apparel textiles. *Color Technol.* **2002**, *118*, 52. [[CrossRef](#)]
32. Raeisi, M.; Kazerouni, Y.; Mohammadi, A.; Hashemi, M.; Hejazi, I.; Seyfi, J.; Khonakdar, H.A.; Davachi, S.M. Superhydrophobic cotton fabrics coated by chitosan and titanium dioxide nanoparticles with enhanced antibacterial and UV-protecting properties. *Int. J. Biol. Macromol.* **2021**, *171*, 158–165. [[CrossRef](#)] [[PubMed](#)]
33. Liu, Z.; Hu, J.; Sun, Q.; Chen, L.; Feng, X.; Zhao, Y. Mussel-inspired multifunctional coating for enhancing the UV-resistant property of polypropylene fibers. *Macromol. Res.* **2017**, *25*, 431–438. [[CrossRef](#)]
34. Vijayalakshmi, K.; Sivaraj, D. Synergistic Antibacterial Activity of Barium Doped TiO<sub>2</sub> Nanoclusters Synthesized by Microwave Processing. *RSC Adv.* **2016**, *6*, 9663–9671. [[CrossRef](#)]
35. Luo, Y.S.; Yang, J.P.; Dai, X.J.; Yang, Y.; Fu, S.Y. Preparation and optical properties of novel transparent Al-doped-ZnO/epoxy nanocomposites. *J. Phys. Chem. C* **2009**, *113*, 9406–9411. [[CrossRef](#)]
36. Kavva, H.V.; Nithin, K.S.; Kendagannaswamy, B.K.; Sachhidananda, S.; Chamaraja, N.A. Optical performance appraisal of mechanically flexible and visibly clear PVP-PVA/calcium doped zirconium oxide nanocomposites for UV shielding applications. *Optik* **2021**, *227*, 166008–166029. [[CrossRef](#)]
37. Arunadevi, R.; Kavitha, B.; Rajarajan, M.; Suganthi, A.; Jeyamurugan, A. Investigation of the drastic improvement of photocatalytic degradation of Congo red by monoclinic Cd, Ba-CuO nanoparticles and its antimicrobial activities. *Surf. Interfaces* **2018**, *10*, 32–44. [[CrossRef](#)]
38. Soumya, S.; Sheemol, V.N.; Amba, P.; Mohamed, A.P.; Ananthakumar, S. Sn and Ag doped ZnO quantum dots with PMMA by in situ polymerization for UV/IR protective, photochromic multifunctional hybrid coatings. *Sol. Energy Mater. Sol. Cells* **2018**, *174*, 554–565. [[CrossRef](#)]
39. Uthirakumar, P.; Devendiran, M.; Yun, J.H.; Kim, G.C.; Kalaiarasan, S.; Lee, I.H. Role of carbon quantum dots and film thickness on enhanced UV shielding capability of flexible polymer film containing carbon quantum dots/N-doped ZnO nanoparticles. *Opt. Mater.* **2018**, *84*, 771–777. [[CrossRef](#)]

**Disclaimer/Publisher’s Note:** The statements, opinions and data contained in all publications are solely those of the individual author(s) and contributor(s) and not of MDPI and/or the editor(s). MDPI and/or the editor(s) disclaim responsibility for any injury to people or property resulting from any ideas, methods, instructions or products referred to in the content.